Tropical circulation and hydrological cycle response to orbital forcing

V. C. Khon,[1,2] W. Park,[3] M. Latif,[3,4] I. I. Mokhov,[1] and B. Schneider[2]

Received 25 May 2012; revised 6 July 2012; accepted 8 July 2012; published 14 August 2012.

[1] The intensity of the two major atmospheric tropical circulations, the Hadley and Walker circulation, has been analyzed in simulations with the Kiel Climate Model (KCM) of the early Eemian and the early Holocene, both warmer climate epochs compared to the late Holocene, or pre-industrial era. The KCM was forced by changes in orbital parameters corresponding to the early and late Holocene (9.5kyr BP and pre-industrial) and the early Eemian (126kyr BP). An intensification of the Southern Hemisphere (SH) winter Hadley cell and a northward extension of its rising branch, the Intertropical Convergence Zone, relative to pre-industrial are simulated for both warm periods. The Walker circulation's rising branch is shifted westward towards the Indian Ocean due to an increased zonal tropical sea surface temperature (SST) gradient across the Indo-Pacific Ocean, which drives enhanced easterlies over this region. The simulated vertically-integrated water vapor transport across the Equator shows the strongest response for the SH winter (boreal summer) Hadley cell over the Pacific Ocean due to an enhanced cross-equatorial SST gradient in the tropical Pacific during the early Holocene and the early Eemian. The orbitally-induced increase of the cross-equatorial insolation gradient in the tropical Pacific leads to a strengthening (weakening) of the wind speed and enhanced (reduced) evaporative cooling over the southern (northern) tropical Pacific, which reinforces the initial radiatively-forced meridional SST gradient change. The increased cross-equatorial insolation gradient in combination with the strong wind-evaporation-SST feedback and changing humidity are important mechanisms to enhance the SH winter Hadley circulation response to orbital forcing. **Citation:** Khon, V. C., W. Park, M. Latif, I. I. Mokhov, and B. Schneider (2012), Tropical circulation and hydrological cycle response to orbital forcing, *Geophys. Res. Lett.*, *39*, L15708, doi:10.1029/2012GL052482.

1. Introduction

[2] The Hadley circulation, a large-scale meridional overturning circulation in the tropical atmosphere, plays a crucial role in the inter-hemispheric heat and water vapor exchange [e.g., *Lindzen and Pan*, 1994; *Oort and Yienger*, 1996; *Cook*, 2004; *Peixoto and Oort*, 1992; *Webster*, 2004; *Gastineau et al.*, 2009]. An intensification of the Southern Hemisphere (SH) winter (boreal summer) Hadley cell leads to enhanced water vapor inflow across the Equator into the Northern Hemisphere (NH) resulting in positive anomalies of precipitation in the NH Tropics. The Walker circulation is a zonal overturning circulation along the Equator and mostly driven by zonal sea surface temperature (SST) gradients. It is most pronounced over the equatorial Pacific Ocean which features a rather strong zonal SST gradient.

[3] A weakening of the large-scale tropical atmospheric circulation under global warming may have substantial consequences for the hydrological cycle [*Held and Soden*, 2006; *Vecchi and Soden*, 2007]. It has been postulated that a weaker rate of precipitation growth ($\sim$2% K^{-1}) under global warming with respect to a growth rate of 7% K^{-1} for the atmospheric water vapor would result from the weakening of the large-scale overturning circulation in the atmosphere. However, it should be noted that whereas changes of atmospheric moisture content follow the Clausius-Clayperon relationship, the global mean precipitation is rather controlled by the surface energy balance [*Allen and Ingram*, 2002]. Moreover, it was shown that the higher ratio between water vapor and precipitation rates implies a larger residence time of water vapor in the atmosphere [e.g., *Khon et al.*, 2010; *Schneider et al.*, 2010b]. According to climate model simulations [*Schneider et al.*, 2010b; *Khon et al.*, 2010], the water vapor residence time may increase, leading to a larger inertia of the atmospheric hydrological cycle in a warmer climate.

[4] In the present study, we use a global climate model to study the warm climate-response of the Hadley and Walker circulation to orbitally-induced insolation forcing during the early Holocene (9.5kyr BP) and Eemian (126kyr BP) compare to the pre-industrial era (late Holocene, 0kyr) and discuss the mechanisms for the changes.

2. Model Experiments and Methods of Analysis

[5] The Kiel Climate Model (KCM) [*Park et al.*, 2009], a coupled atmosphere–ocean-sea ice general circulation model, is used to simulate the pre-industrial and the past two warm periods, the Holocene and Eemian. The KCM consists of the atmospheric general circulation model, ECHAM5 [*Roeckner et al.*, 2003] with a horizontal resolution of T31 (3.75° × 3.75°) and 19 vertical levels and the ocean-sea ice model, NEMO [*Madec*, 2006] with a horizontal resolution of 2° × 2° and enhanced meridional resolution of 0.5° close to the Equator. The model was shown to realistically simulate present-day climate and further details can be found in *Park et al.* [2009]. Here we analyze three time-slice simulations,

[1]A.M. Obukhov Institute of Atmospheric Physics, Russian Academy of Sciences, Moscow, Russia.
[2]Institute of Geosciences, Kiel University, Kiel, Germany.
[3]Helmholtz Centre for Ocean Research Kiel (GEOMAR), Kiel, Germany.
[4]Cluster of Excellence "The Future Ocean", Kiel University, Kiel, Germany.

Corresponding author: V. C. Khon, A.M. Obukhov Institute of Atmospheric Physics, Russian Academy of Sciences, Pyzhevsky 3, 119017 Moscow, Russia. (khon@ifaran.ru)

0094-8276/12/2012GL052482

which were performed using different orbital configurations [*Braconnot et al.*, 2008] corresponding to distinct time periods during the Holocene and Eemian epochs [*Schneider et al.*, 2010a; *Khon et al.*, 2010]. *Schneider et al.* [2010a] compared the model's temperature trends during the Holocene with proxy data. Further details on the orbital configurations are given in *Khon et al.* [2010]. The atmospheric CO_2 concentration was fixed to the pre-industrial level of 286.2 ppm. We analyzed the last 100 years of the 1000 years long integrations which were started from Levitus' climatology.

[6] The tendency of SST (T') as a function of time can be considered through the vertical integration of the heat balance equation for the ocean mixed layer [e.g., *Dong et al.*, 2007]:

$$\frac{\partial T}{\partial t} \equiv T' = \frac{1}{\rho c_p H}(Q + HT), \quad (1)$$

where $\rho c_p = 4.1\ 10^6$ J m^{-3} K^{-1} is the ocean density times the seawater specific capacity; H is the mixed layer depth (MLD); $Q = SW + LW + SH + LH - I$ is the net heat flux composed of surface shortwave (SW) and longwave (LW) radiation, sensible (SH) and latent (LH) heat fluxes, and downward radiative flux (I) at the mixed layer base, $HT = -\rho c_p \int_{-H}^{0} \vec{u} \cdot \nabla T dz$ is heat transport by ocean currents vertically integrated over the depth of mixed layer (MLD). To calculate I we used the following approximation [*Manizza et al.*, 2005]: $I = SW \cdot (0.58e^{-K_{IR}H} + 0.42e^{-K_{VIS}H})$, where $K_{IR} = 2.86$ m^{-1} and $K_{VIS} = 0.0434$ m^{-1} represent the light attenuation coefficients for irradiance and visible light band, respectively.

3. Response of the Hadley and Walker Circulation to Orbital Forcing During the Early Holocene and the Early Eemian

[7] The zonal-mean meridional streamfunctions for the early Holocene (9.5kyr BP) and the early Eemian (126kyr BP) simulations and their difference to the preindustrial mean obtained from a pre-industrial control integration (0 K) are shown in Figures 1a and 1b for the SH winter (JJA). The model results depict a strengthening of the SH winter Hadley cell and a northward extension of its rising branch, the Intertropical Convergence Zone (ITCZ), during the both epochs. The early Holocene and the early Eemian changes in the SH winter Hadley cell strength (measured by an absolute maximum of streamfunction within the tropics) amount to about 10% and 13%, respectively (Figure 1c). A northward movement by 2–3 degrees of the zonal-mean ITCZ position is also found which was calculated as the latitude of the zero-streamline within the northern Tropics at 500 hPa (not shown). In contrast, during boreal winter, the model does not simulate any significant changes in the mean meridional overturning circulation, neither in 9.5kyr nor in 126kyr BP (not shown). We therefore concentrate in the following on the SH winter.

[8] The intensification of the SH winter Hadley cell leads to a stronger northward water vapor transport. We use the atmospheric water vapor transport across the Equator at three different longitude bands to investigate the regional changes of the Hadley circulation strength [see also *Oort and Yienger*, 1996]: the Atlantic (70°W–25°E), Indian Ocean (25°–125°E) and Pacific (125°E–70°W) Sectors (Figure 1c). The northward cross-equatorial surface flow is strengthened over the Atlantic, and especially over the Pacific Sector, whereas the Indian Ocean Sector does not exhibit any strong changes. Over the Atlantic, the model simulates an enhanced meridional SST gradient, with warmer SST to the north of 10°N and colder SST to the south (Figures 2a and 2b). This dipole structure - which is attributed to the enhanced insolation gradient and the local positive wind-evaporation-SST (WES) feedback [see *Zhao et al.*, 2005] - results in a stronger meridional circulation in the northern tropical Atlantic region and also a northward extension of the SH Hadley cell over Atlantic during the early Holocene and the early Eemian.

[9] The result that the Hadley circulation over the Indian Ocean is only slightly affected by the insolation forcing has been previously reported in several papers [*Liu et al.*, 2003; *Ohgaito and Abe-Ouchi*, 2007; *Braconnot et al.*, 2007; *Marzin and Braconnot*, 2009]. However, our model results also reveal a strengthening of a zonal (Walker-type) circulation over the Indo-Pacific region. The changes in SST, wind vectors (a, b), and the associated anomalies of the zonal overturning circulation (c, d) over the equatorial Pacific are shown in Figure 2 for the early Holocene (a, c) and the early Eemian (b, d). To eliminate a possible contribution of the meridional (Hadley-type) circulation we analyzed the deviation of the velocity potential from its zonal mean [see *Tanaka et al.*, 2004]. The corresponding changes in the non-zonal mean component of the 200 hPa velocity potential are shown in Figures 2c and 2d for the early Holocene and the early Eemian, respectively. The model shows the early Holocene and Eemian increase in the zonal SST gradient across the Indo-Pacific Ocean, with maximum cooling over the central Equatorial Pacific and warming over the tropical Indian Ocean. This strengthens the easterly winds over the Indo-Pacific region during the early Holocene and, especially, during the early Eemian with stronger zonal SST gradient in this region (Figures 2a and 2b). As a result, the simulated longitudinal location of the rising branch of the Walker circulation is shifted from the Pacific warm pool westward towards the Indian Ocean during boreal summer (Figures 2c and 2d). The estimated westward extension of the Walker circulation amounts to about 15° for the early Holocene and about 20° for the early Eemian (with stronger zonal temperature gradient across the Indo-Pacific Ocean).

[10] It should be noted that the stronger easterlies over Indo-Pacific region during the early Holocene and the early Eemian weaken the summer monsoonal flow over the Bay of Bengal, and they appear to reduce the impact of the direct solar radiation on the Asian monsoon [see, e.g., *Liu et al.*, 2004; *Zhao et al.*, 2005].

4. Possible Mechanisms for the Intensified Hadley Circulation

[11] The surface wind speed and the evaporation during the early Holocene and the early Eemian are compared to those of the pre-industrial era (Figures 3a and 3b). During the SH winter, the primarily orbitally-induced increase of the cross-equatorial insolation gradient in the tropical Pacific (Figures 4a and 4c) drives enhanced southerly winds

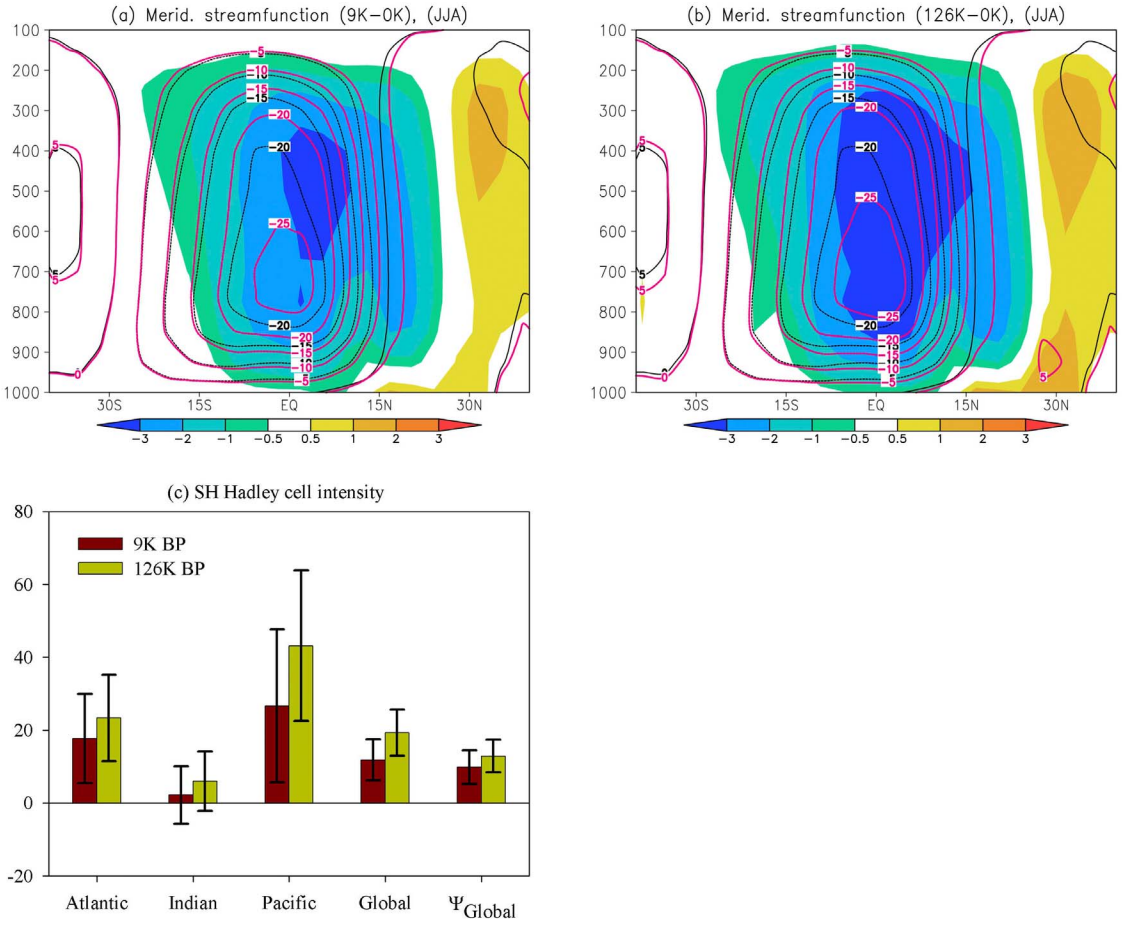

Figure 1. Changes (shaded) in the boreal summer meridional streamfunction (10^{10} kg s^{-1}) for (a) early Holocene (9.5 K minus 0 K) and (b) Eemian (126 K minus 0 K) simulations. Red contours show mean streamfunctions for Figure 1a. 9.5 K and (b) 126 K simulations in comparison to pre-industrial (black contours). The positive (negative) value of streamfunction corresponds to a clockwise (counterclockwise) circulation. (c) Regional changes (%) in vertically-integrated northward water vapor transport across the equator (averaged over latitudinal band 10°S–10°N) for 9.5 K and 126 K (relative to pre-industrial) during boreal summer: Atlantic (70°W–25°E), Indian (25°–125°E), Pacific (125°E–70°W) sector and total zonal-mean transport across the equator. Changes in the maximum value of the zonal-mean meridional streamfunction are also presented.

(Figures 2a and 2b) which cross the Equator. The stronger southeasterly wind in the southern tropical Pacific leads to enhanced evaporative cooling (Figures 3a and 3b; contours) and, as a consequence, to colder SST in this region (Figures 2a and 2b). The basin-wide cooling over the southern tropical Pacific will facilitate a further amplification of the primary cross-equatorial SST gradient. Conversely, stronger westerly winds in the northeastern tropical Pacific weaken the trade winds and hence lead to higher SSTs there (Figures 2a and 2b). This positive wind-evaporation-SST (WES) feedback causes a stronger inter-hemispheric asymmetry [e.g., *Xie and Philander*, 1994; *Xie*, 2004], which in particular leads to a weakening of the South Pacific Convergence Zone (SPCZ) and a strengthening of its Northern Hemisphere counterpart during the early Holocene and the early Eemian (Figures 3c and 3d). This effect dominates the annual mean response, exhibiting positive (negative) precipitation anomalies in the Northern (Southern) Hemisphere during the early Holocene and the early Eemian (not shown).

[12] For a given time interval (e.g., season), the change (with respect to 0 K) in the warming rate (T') may be decomposed into components due to heat fluxes (T'_Q), mixed layer depth (T'_{MLD}) and ocean heat transport (T'_{HT}) vertically integrated over the MLD:

$$\delta T' = \delta T'_Q + \delta T'_{HT} + \delta T'_{MLD},$$

where

$$\delta T'_Q = \frac{1}{\rho c_p H_{0K}}(\delta SW + \delta LW + \delta SH + \delta LH - \delta I),$$

$$\delta I = \frac{I_{0K}}{SW_{0K}}\delta SW, \delta T'_{HT} = \frac{\delta HT}{\rho c_p H_{0K}}.$$

The effect of the MLD on the SST tendency may be estimated as a residual term:

$$\delta T'_{MLD} = \delta T' - \delta T'_Q - \delta T'_{HT}.$$

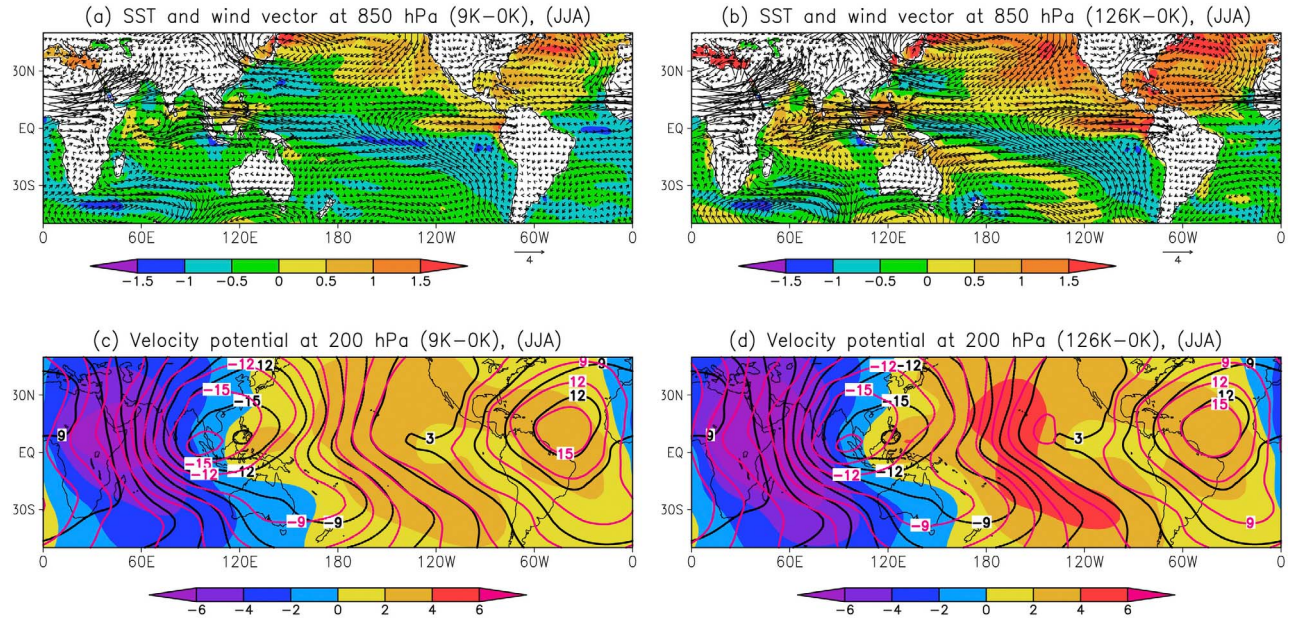

Figure 2. Simulated (a, c) Holocene and (b, d) Eemian changes for SST (shaded) and 850 hPa wind (arrows) (Figures 2a and 2b), non-zonal component of 200 hPa velocity potential (shaded) (Figures 2c and 2d) for the early Holocene (Figures 2a and 2c) and the early Eemian (Figures 2b and 2d). Red contours in Figures 2c and 2d show mean non-zonal components of 200 hPa velocity potential [$10^6 m^2 s^{-1}$] for 9.5 K (Figure 2c) and 126 K (Figures 2d) in comparison to 0 K (black contours) simulation.

The northern tropical Pacific (a region with strong WES feedback) SST tendencies computed from the heat balance equation (1) for 0 K are in a good agreement with those calculated from the model output SST (Figure 4c). The individual terms $\delta T_i'$ for both the early Holocene and the early Eemian are shown in Figure 4d. The SW term in Figure 4d implies a contribution caused by difference between surface and mixed layer base SW radiation. According to the model results, a major contribution to $\delta T'$ over the northern tropical Pacific during the early Holocene is due to changes in the latent heat flux (∼70% of total warming rate change), while the contributions of the radiative fluxes and the MLD term amount to ∼10% and ∼20%, respectively. The contribution of the sensible heat flux is

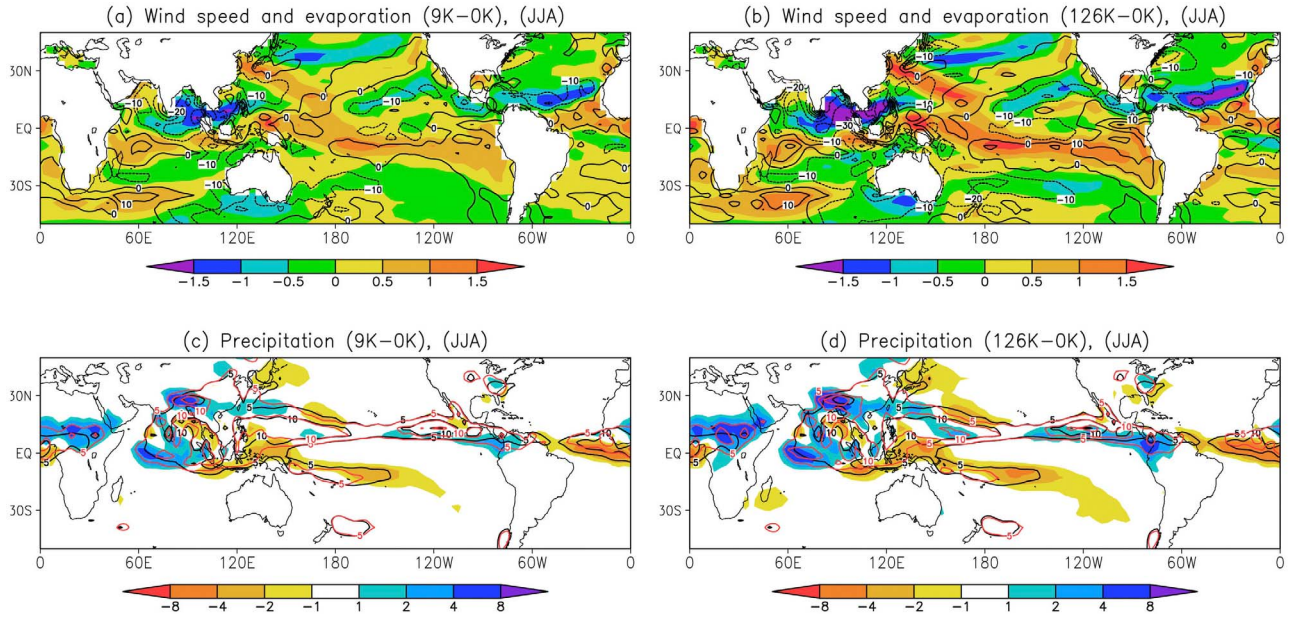

Figure 3. Simulated (a, c) the early Holocene and (b, d) the early Eemian changes for wind speed (shaded) and evaporation (contours) (Figures 3a and 3b), precipitation (shaded) during boreal summer (Figures 3c and 3d). Red contours in Figures 3c and 3d show mean precipitation for 9.5 K (Figure 3c) and 126 K (Figure 3d) in comparison to 0 K (black contours) simulation.

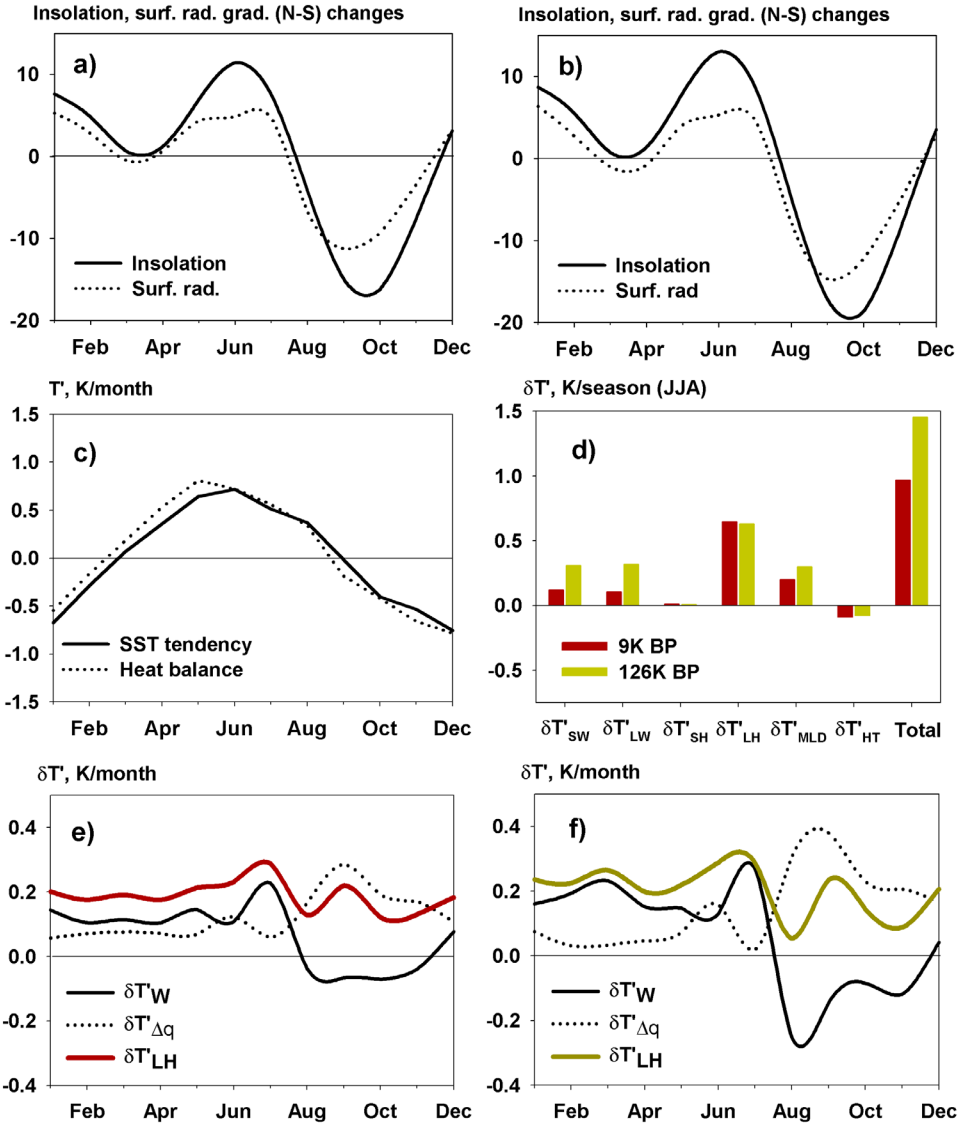

Figure 4. Changes in cross-equatorial gradient (North minus South) of insolation (Wm^{-2}) and net surface radiation (Wm^{-2}) for (a) 9 K and (b) 126 K simulations in the tropical Pacific, in which the area mean of the quantities are taken over the southern (20ºS–7.5ºS; 180°–100°W) and northern (7.5°N–20°N; 180°–100°W) area. (c) Monthly mean SST tendency (T') for 0 K in comparison to that calculated from heat balance equation. (d) Decomposition of T' changes into components due to changes in shortwave ($\delta T'_{SW}$) and longwave ($\delta T'_{LW}$) radiation, sensible ($\delta T'_{SH}$) and latent heat ($\delta T'_{LH}$), mixed layer depth ($\delta T'_{MLD}$) and ocean heat transport ($\delta T'_{HT}$) for 9 K and 126 K simulations. (e, f) Monthly mean $\delta T'_{LH}$ and its decomposition into wind ($\delta T'_{W}$) and humidity ($\delta T'_{\Delta q}$) terms. All the results in Figures 4c–4f are shown for the northern tropical Pacific (7.5°N–20°N; 180°W–100°W).

negligible. However, for the early Eemian exhibiting a higher warming rate change relative to 9 K, the model depicts a less significant LH contribution (~45%) and larger relative contributions of SW and LW to $\delta T'$. As the latent heat flux is a function of the surface wind speed and the humidity gradient, we further decompose the LH-related changes into contributions from wind speed (δLH_W) and humidity ($\delta LH_{\Delta q}$) changes using standard bulk formula [e.g., *Du and Xie*, 2008]:

$$\delta LH = \delta LH_W + \delta LH_{\Delta q},$$

where

$$\delta LH_W = \frac{LH_{0K}}{W_{0K}}\delta W,$$

W is the surface wind speed. Hence, changes in the warming rate due to wind speed variations may be written as

$$\delta T'_W = \frac{1}{\rho c_p H_{0K}}\frac{LH_{0K}}{W_{0K}}\delta W.$$

The humidity term was calculated as follows

$$\delta T'_{\Delta q} = \delta T'_{LH} - \delta T'_W.$$

The intra-seasonal variations of $\delta T'_W$ and $\delta T'_{\Delta q}$ for both the early Holocene and the early Eemian are shown in Figures 4e and 4f. The strong orbitally-induced increase of the cross-equatorial insolation gradient during June–July (Figures 4a and 4b) leads to higher $\delta T'_W$ and $\delta T'_{LH}$ in the northern tropical Pacific via a strong wind-evaporation link, while the humidity term is relatively small (Figures 4e and 4f). Conversely, the reduced insolation gradient during August–September (Figures 4a and 4b) causes positive surface wind speed anomalies in the northern tropical Pacific (and negative $\delta T'_W$). However, this wind-induced cooling is overpowered by the warming due to enhanced relative humidity (Figures 4e and 4f) during both epochs.

5. Summary and Conclusions

[13] We analyze simulations of the early Holocene (9.5 K) and the early Eemian warm period (126 K) with respect to the pre-industrial era (0 K) with the Kiel Climate Model (KCM). The model simulates an intensification of the SH winter (boreal summer) Hadley cell and a northward extension of its rising branch (ITCZ) for both the early Holocene and the early Eemian. The strengthening of the Hadley circulation dominates over the tropical Atlantic and, especially, over the tropical Pacific Sectors and is forced by an enhanced meridional SST gradient between the southern and the northern Tropics.

[14] The enhanced orbitally-induced cross-equatorial insolation gradient drives cross-equatorial southerly winds during the early summer (June–July), thereby reducing the wind speed and evaporative cooling over the northern tropical Pacific. This reinforces the initial meridional SST gradient perturbation directly driven by the insolation change. During the late summer (August–September), the positive changes in $\delta T'_{LH}$ can be attributed to enhanced humidity ($\delta T'_{\Delta q} > 0$), which overcomes the wind-induced cooling ($\delta T'_W < 0$) over the northern tropical Pacific for these months during both the early Holocene and the early Eemian. We also show that the rising branch of the Walker circulation is shifted towards the Indian Ocean during the early Holocene and the early Eemian in response to an increased zonal SST gradient across the Indo-Pacific Ocean. Finally, the WES feedback promotes a stronger inter-hemispheric asymmetry, leading to a weakening of the South Pacific Convergence Zone (SPCZ) and to a strengthening of its northern counterpart during the early Holocene and the early Eemian.

[15] **Acknowledgments.** This work was supported by the Excellence Cluster "Future Ocean", the Sonderforschungsbereich SFB754, German Priority Research Program SPP 1266 (INTERDYNAMIK) and the Ministry of Education and Science of the Russian Federation (contract 14.740.11.1043). The model integrations were performed at the Computer Centre at Kiel University.

[16] The Editor thanks the anonymous reviewer for assisting in the evaluation of this paper.

References

Allen, M., and W. Ingram (2002), Constraints on future changes in climate and the hydrologic cycle, *Nature*, *419*, 224–232, doi:10.1038/nature01092.

Braconnot, P., et al. (2007), Results of PMIP2 coupled simulations of the mid-Holocene and Last Glacial Maximum—Part 2: Feedbacks with emphasis on the location of the ITCZ and mid- and high-latitudes heat budget, *Clim. Past*, *3*(2), 279–296, doi:10.5194/cp-3-279-2007.

Braconnot, P., C. Marzin, L. Gregoire, E. Mosquet, and O. Marti (2008), Monsoon response to changes in Earth's orbital parameters: Comparisons between simulations of the Eemian and of the Holocene, *Clim. Past*, *4*, 281–294, doi:10.5194/cp-4-281-2008.

Cook, K. H. (2004), Hadley circulation dynamics: Seasonality and the role of continents, in *The Hadley Circulation: Present, Past and Future*, edited by H. F. Diaz and R. S. Bradley, pp. 61–83, Springer, New York, doi:10.1007/978-1-4020-2944-8_2.

Dong, S., S. T. Gille, and J. Sprintall (2007), An assessment of the Southern Ocean mixed layer heat budget, *J. Clim.*, *20*(17), 4425–4442, doi:10.1175/JCLI4259.1.

Du, Y., and S.-P. Xie (2008), Role of atmospheric adjustments in the tropical Indian Ocean warming during the 20th century in climate models, *Geophys. Res. Lett.*, *35*, L08712, doi:10.1029/2008GL033631.

Gastineau, G., H. Le Treut, and L. Li (2009), The Hadley and Walker circulation changes in global warming conditions described by idealized atmospheric simulations, *J. Clim.*, *22*, 3993–4013, doi:10.1175/2009JCLI2794.1.

Held, I., and B. Soden (2006), Robust response of the hydrological cycle to global warming, *J. Clim.*, *19*, 5686–5699, doi:10.1175/JCLI3990.1.

Khon, V. C., W. Park, M. Latif, I. I. Mokhov, and B. Schneider (2010), Response of the hydrological cycle to orbital and greenhouse gas forcing, *Geophys. Res. Lett.*, *37*, L19705, doi:10.1029/2010GL044377.

Lindzen, R. S., and W. Pan (1994), A note on orbital control of equator-pole heat fluxes, *Clim. Dyn.*, *10*, 49–57, doi:10.1007/BF00210336.

Liu, Z., et al. (2003), Coupled climate simulation of the evolution of global monsoons in the Holocene, *J. Clim.*, *16*(15), 2472–2490, doi:10.1175/1520-0442(2003)016<2472:CCSOTE>2.0.CO;2.

Liu, Z., S. P. Harrison, J. Kutzbach, and B. Otto-Bliesner (2004), Global monsoons in the mid-Holocene and oceanic feedback, *Clim. Dyn.*, *22*, 157–182, doi:10.1007/s00382-003-0372-y.

Madec, G. (2006), NEMO reference manual, ocean dynamics component: NEMO-OPA. Preliminary version, *Note Pole Model. 27*, Inst. Pierre-Simon Laplace, Paris.

Manizza, M., C. Le Quéré, A. J. Watson, and E. T. Buitenhuis (2005), Bio-optical feedbacks among phytoplankton, upper ocean physics and sea-ice in a global model, *Geophys. Res. Lett.*, *32*, L05603, doi:10.1029/2004GL020778.

Marzin, C., and P. Braconnot (2009), The role of the ocean feedback on Asian and African monsoon variations at 6 kyr and 9.5 kyr BP, *C. R. Geosci.*, *341*(8–9), 643–655, doi:10.1016/j.crte.2009.09.001.

Ohgaito, R., and A. Abe-Ouchi (2007), The role of ocean thermodynamics and dynamics in Asian summer monsoon changes during the mid-Holocene, *Clim. Dyn.*, *29*(1), 39–50, doi:10.1007/s00382-006-0217-6.

Oort, A., and J. Yienger (1996), Observed interannual variability in the Hadley circulation and its connection to ENSO, *J. Clim.*, *9*, 2751–2767, doi:10.1175/1520-0442(1996)009<2751:OIVITH>2.0.CO;2.

Park, W., N. Keenlyside, M. Latif, A. Stroeh, R. Redler, E. Roeckner, and G. Madec (2009), Tropical Pacific climate and its response to global warming in the Kiel Climate Model, *J. Clim.*, *22*, 71–92, doi:10.1175/2008JCLI2261.1.

Peixoto, J., and A. Oort (1992), *Physics of Climate*, 520 pp., Am. Inst. of Phys., New York.

Roeckner, E., et al. (2003), The atmospheric general circulation model ECHAM 5. Part I: Model description, *Rep. 349*, Max Planck Inst. for Meteorol., Hamburg, Germany.

Schneider, B., G. Leduc, and W. Park (2010a), Disentangling seasonal signals in Holocene climate trends by satellite-model-proxy integration, *Paleoceanography*, *25*, PA4217, doi:10.1029/2009PA001893.

Schneider, T., P. O'Gorman, and X. Levine (2010b), Water vapor and the dynamics of climate changes, *Rev. Geophys.*, *48*, RG3001, doi:10.1029/2009RG000302.

Tanaka, H. L., N. Ishizaki, and A. Kitoh (2004), Trend and interannual variability of Walker, monsoon and Hadley circulations defined by velocity potential in the upper troposphere, *Tellus, Ser. A*, *56*, 250–269.

Vecchi, G. A., and B. J. Soden (2007), Global warming and the weakening of the tropical circulation, *J. Clim.*, *20*, 4316–4340, doi:10.1175/JCLI4258.1.

Webster, P. J. (2004), The elementary Hadley circulation, in *The Hadley Circulation: Present, Past and Future*, edited by H. F. Diaz and R. S. Bradley, pp. 9–60, Springer, New York, doi:10.1007/978-1-4020-2944-8_1.

Xie, S.-P. (2004), The shape of continents, air-sea interaction, and the rising branch of the Hadley circulation, in *The Hadley Circulation: Present, Past and Future*, edited by H. F. Diaz and R. S. Bradley, pp. 121–152, Springer, New York, doi:10.1007/978-1-4020-2944-8_4.

Xie, S.-P., and S. G. H. Philander (1994), A coupled ocean–atmosphere model of relevance to the ITCZ in the eastern Pacific, *Tellus, Ser. A*, *46*, 340–350.

Zhao, Y., P. Braconnot, O. Marti, S. P. Harrison, C. Hewitt, A. Kitoh, Z. Liu, U. Mikolajewicz, B. Otto-Bliesner, and S. L. Weber (2005), A multi-model analysis of the role of the ocean on the African and Indian monsoon during the mid-Holocene, *Clim. Dyn.*, *25*, 777–800, doi:10.1007/s00382-005-0075-7.